Clays and Clay Minerals, Vol. 57, No. 6, 715–724, 2009.

BIRNESSITES WITH DIFFERENT AVERAGE MANGANESE OXIDATION STATES SYNTHESIZED, CHARACTERIZED, AND TRANSFORMED TO TODOROKITE AT ATMOSPHERIC PRESSURE

HAOJIE CUI[1,2], GUOHONG QIU[1], XIONGHAN FENG[1], WENFENG TAN[1], AND FAN LIU[1,*]

[1] Key Laboratory of Subtropical Agricultural Resources and Environment, Ministry of Agriculture, Huazhong Agricultural University, Wuhan 430070, China

[2] Institute of Urban Environment, Chinese Academy of Sciences, Xiamen 361021, China

Abstract—Todorokite is a common manganese oxide mineral, with a tunnel structure, found in Earth surface environments, and is easily synthesized from layered birnessite. The aim of the current study was to prepare birnessites with different average manganese oxidation states (AOS) by controlling the MnO_4^-/Mn^{2+} ratio in concentrated NaOH or KOH. A series of (Na,K)-birnessites, Na-birnessites, and K-birnessites with different AOS was synthesized successfully in strongly alkaline media. The (Na,K)-birnessites and Na-birnessites prepared in NaOH clearly contained both large (500−1000 nm) and small (40−400 nm), plate-shaped crystallites. The K-birnessites prepared in KOH media consisted mostly of irregular (100−200 nm), plate-shaped crystallites. The degree of transformation of birnessite to todorokite at atmospheric pressure decreased as the AOS values of (Na,K)-birnessites and Na-birnessites increased from 3.51 to 3.80. No todorokite was present when a Na-birnessite with an AOS value of 3.87 was used as the precursor. Pyrophosphate, which is known to form strong complexes with Mn^{3+} at a pH range of 1−8, was added to a suspension of (Na,K)-birnessites in order to sequester the available Mn^{3+} in (Na,K)-birnessites. Removal of Mn^{3+} from birnessite MnO_6 layers by pyrophosphate restricted transformation to todorokite − no (Na,K)-birnessite transformed to todorokite after pyrophosphate treatment. The interlayer K^+ initially within (Na,K)-birnessites could not be completely ion-exchanged with Mg^{2+} to form todorokite at atmospheric pressure. No todorokite was forthcoming from K-birnessites even from those with small AOS values (3.50).

Key Words—AOS, Atmospheric Pressure, Birnessite, Todorokite.

INTRODUCTION

Manganese oxide minerals are ubiquitous in soils and sediments and participate in a wide variety of chemical reactions, such as oxidation-reduction and cation-exchange reactions, which affect the compositions and chemical behaviors of sediments and soils and associated aqueous systems (Post, 1999). The todorokites are a group of manganese oxide minerals with large tunnels and a 3×3 array of edge-shared MnO_6 octahedra. Todorokites have been studied extensively for particular properties which make them suitable for use as ion sieves, molecular sieves, catalysts, and cathode materials for lithium batteries (Turner *et al.*, 1982; Golden *et al.*, 1986; Post, 1999; Shen *et al.*, 1993; Zhou *et al*., 1998; Al-Sagheer and Zaki, 2004; Kumagai *et al*., 2001). Todorokite is commonly synthesized from birnessite, the layer-structured precursor, in the following three steps: birnessite → buserite → todorokite. Todorokite was first synthesized, under hydrothermal conditions, by Golden *et al.* (1986), through autoclave treatment of Mg^{2+}-exchanged birnessite (Mg-buserite). Other hydrated inorganic divalent cations, such as Ni^{2+}, Co^{2+}, and Cu^{2+}, have been used successfully in templates for the synthesis of todorokites with different physical and chemical properties (Golden *et al.*, 1987; Shen *et al.*, 1994). More than 25 kinds of metal ions have been exchanged into stabilized Na-buserite by a double-aging method and the resultant metal-buserites were used successfully to prepare todorokites by hydrothermal treatment (Luo *et al.*, 1999). The crystallinity, thermal stability, and particle morphology of the synthetic todorokites were related to the crystallinity of the initial Na-birnessite (Liu *et al.*, 2005). Almost all of the todorokites noted above were synthesized under hydrothermal conditions in an autoclave at a relatively high temperature and pressure and the synthetic todorokites differed only in the initial birnessite and the type of metal that was introduced into the interlayer. Feng *et al*. (2004) first synthesized todorokite at atmospheric pressure by refluxing (100ºC) Mg-buserite and found that the product structure and other characteristics were similar to those of hydrothermally synthesized samples. The Feng *et al*. (2004) study provided a more convenient means by which to explore the factors and mechanisms of todorokite formation at atmospheric pressure. Examination of factors and conditions influencing todorokite formation at atmospheric pressure could have great significance in future understanding of the mechanisms of formation of todorokite in nature.

* E-mail address of corresponding author:
liufan@mail.hzau.edu.cn
DOI: 10.1346/CCMN.2009.0570605

The formation of todorokite and the initial birnessite are closely associated. Atmospheric pressure and the characteristics of precursor birnessites, which were formed in different environments, might affect the formation of todorokite, however (Cui *et al*., 2005, 2006). Oxidation of the Mn^{2+} located above or below vacant sites facilitated the formation of a stable todorokite-like structure during marine diagenesis and hydrothermal treatment (Mellin and Lei, 1993). During hydrothermal heat treatment, some octahedral Mn(III) from the buserite layers could migrate into the interlayer and become corner-sharing octahedra that assist in tunnel 'wall' formation (Liu *et al.*, 2002). Todorokite can be prepared easily by hydrothermal treatment of Cu-buserite and Co-buserite at high temperature (150−170ºC) (Shen *et al*., 1993). However, the Cu- and Co-buserites could not be converted into todorokite by refluxing at atmospheric pressure because Cu^{2+} and Co^{2+} bond tightly to MnO_6 layers *via* shorter bonds (Cu−O or Co−O) by replacement of interlayer Mn^{2+} located above or below octahedral vacancies (Cui *et al*., 2005). Recent work (Cui *et al.*, 2008, 2009) has shown that the formation of todorokite is closely related to the Mn(III) content or to MnO_6 octahedral vacancies. The number of Mn(III) or vacant sites in birnessite depends partly on the average manganese oxidation state (AOS). Greater numbers of vacant sites were present in birnessites with larger AOS values. Pyrophosphate is known to form strong complexes with Mn(III) at a pH range of 1−8. The availability of Mn(III) for phase transformation from layered to tunnel-structured manganese oxide can be predicted by Mn(III) complexation with pyrophosphate. A series of todorokite synthesis efforts, using different cations as templates, indicated that cation type affects the physicochemical properties of todorokite. Although many studies have examined the synthesis of todorokite, no report was found that examines the effect of the birnessite interlayer cation on the formation of todorokite at atmospheric pressure. The formation of todorokite from birnessites with different AOS values at atmospheric pressure was, therefore, the focus of the current investigation. The birnessites were prepared by oxidation of aqueous Mn^{2+} in concentrated NaOH or KOH with different MnO_4^-/Mn^{2+} ratios. The effects of the interlayer cation of the birnessite on the formation of todorokite was investigated using three different types of birnessites which contained interlayer K^+, Na^+, or both Na^+ and K^+ cations. Results from this study are expected to shed light on the mechanisms of formation of todorokite in Earth surface environments.

MATERIALS

Preparation of birnessites with different AOS values

A solution of 44 g of NaOH (1.1 moles) in 125 mL of distilled-deionized water (DDW) was quickly added to a solution of 9.066 g of $MnCl_2{\cdot}4H_2O$ (0.045 moles) in 125 mL of DDW under vigorous stirring to form a white $Mn(OH)_2$ slurry. A solution containing 3.982 g of $KMnO_4$ (0.025 moles) in 250 mL of DDW was added dropwise to the slurry under vigorous stirring to produce a brownish-black suspension of MnO_x. The reaction mixture was stirred for another 30 min and aged at 60ºC for 12 h. The product was then filtered and washed until the filtered solution was ~pH 7. The washed samples were named 0.55-(Na,K)-bir, for example, where 0.55 was the $KMnO_4/Mn^{2+}$ ratio. The 0.45-(Na,K)-bir and 0.33-(Na,K)-bir syntheses were similar to the 0.55-(Na,K)-bir synthesis, except that 11.081 g (0.056 moles) and 14.960 g (0.075 moles), respectively, of $MnCl_2{\cdot}4H_2O$ were added, to yield $KMnO_4/Mn^{2+}$ ratios of 0.45 and 0.33, respectively.

Synthesis of Na-birnessites was similar to that of (Na,K)-birnessites, but $NaMnO_4{\cdot}H_2O$ (Sigma Aldrich Co., St. Louis, Missouri) was used as the oxidant and the $NaMnO_4/Mn^{2+}$ ratios were 0.33, 0.45, and 0.55. The washed samples were designated 0.33-Na-bir, 0.45-Na-bir, and 0.55-Na-bir, respectively. Synthesis of the K-birnessite was similar to that of the (Na,K)-birnessite, but KOH solution was used instead of NaOH. The washed samples were designated 0.33-K-bir, 0.45-K-bir, and 0.55-K-bir, respectively.

Pyrophosphate treatment of (Na,K)-birnessite and Mn(III)-pyrophosphate-complex measurement

Samples (2 g) of each of three types of (Na,K)-birnessites were dispersed in 200 mL of pH 7 0.01 M and 0.02 M $Na_4P_2O_7$ solutions. After mild stirring for 12 h, the suspensions were centrifuged. The solutions were saved for Mn(III)-pyrophosphate-complex measurements and the solids were washed 3−5 times with DDW. The concentration of Mn(III) complex was determined using a visible spectrophotometer (vis-7220 model (Double Beam Models/UV-6300 (PC), Shanghai Mapada Instruments Co. Ltd., China) at 482 nm (Cui *et al*., 2008).

Mg^{2+}-reflux treatment: $MgCl_2$ treatment of birnessite and subsequent conversion to todorokite

The prepared birnessites were dispersed in 400 mL of 0.5 M $MgCl_2$ solutions. After gentle stirring for 12 h, the suspensions were centrifuged and the solids washed 3−5 times with DDW. The products were dispersed in 350 mL of DDW, and the suspensions transferred to flasks and refluxed (100ºC) with stirring for 24 h at atmospheric pressure. The refluxed products were washed 3−5 times using DDW and then dried.

ANALYTICAL METHODS

Elemental analysis, AOS determination, and infrared (IR) analyses

To determine the elemental composition, 150 mg of sample was dissolved in 50 mL of aqua regia and diluted

https://doi.org/10.1346/CCMN.2009.0570605 Published online by Cambridge University Press

to 1000 mL. The Na, K, Mg, and Mn contents were analyzed using a Varian Vista-MPX ICP-OES instrument. The AOS of the birnessite samples was measured by the oxalic acid-permanganate back-titration method. Briefly, 0.1 g of the sample was completely dissolved in 10 mL of 0.5 M $H_2C_2O_4$ and 10 mL of 0.5 M H_2SO_4 to reduce all of the manganese to Mn^{2+}. The extra $C_2O_4^{2-}$ was determined by back-titration at 60ºC with standardized 0.02 M $KMnO_4$ solution. The AOS was calculated on the basis of both the titration result and the total amount of Mn determined by inductively coupled plasma-mass spectrometry (ICP-MS) (Feng *et al.*, 2004). All mid-IR (infrared) spectra were obtained using a VERTEX 70 model spectrophotometer with KBr pellets (sample:KBr = 1:400), with a setting of 15 scans/spectrum over the range 4000−400 cm^{-1} at a resolution of 4 cm^{-1}.

X-ray diffraction studies

X-ray diffraction (XRD) scans were performed at ambient temperature using a D/Max-3B diffractometer equipped with monochromated FeKα radiation (λ = 0.1937 nm) or CuKα radiation (λ = 0.1541 nm). The diffractometer was operated at a tube voltage of 40 kV, a tube current of 20 mA, and a step scanning rate of 0.02º per 0.5 s.

Transmission electron microscopy measurements

The samples were crushed gently to a powder, dispersed ultrasonically in absolute alcohol, deposited on a holey copper grid, and dried in air. The transmission electron microscopy (TEM) images were obtained using a JEOL JEM 2010 instrument at an accelerating voltage of 200 kV. High resolution-TEM (HRTEM) was performed using a JEOL JEM 2010 FEF electron microscope operated at 200 kV.

RESULTS

Characterization of synthetic birnessites

The XRD patterns of the various synthetic birnessites had peaks at *d* spacings of 0.72, 0.36, 0.24, and 0.23 nm (Figure 1) indicating that the birnessites were pure. Experimental measurements of the elemental compositions and AOS values of the synthetic birnessite samples (Table 1) revealed that the Na^+ concentrations in three types of (Na,K)-birnessites was unaffected, whereas the K^+ concentrations increased with larger $KMnO_4/Mn^{2+}$ ratios. The Na^+ contents were considerably greater than the K^+ contents in these synthetic birnessites. The Na contents of three types of Na-birnessites were comparable to those of the (Na,K)-birnessites and the K^+ contents of three types of K-birnessites ranged from 0.61 to 1.11 mmol/g depending on the $KMnO_4/Mn^{2+}$ ratio. The Mn content of the birnessites prepared in different media decreased and the AOS values increased with increased $KMnO_4/Mn^{2+}$ ratio.

The TEM images of the (Na,K)-birnessites and the Na-birnessites and Na-birnessites consist of large (500−1000 nm) platelets and small (40−400 nm) platelets (Figure 2a−f), but the K-birnessites consist mostly of irregular, plate-shaped (100−200 nm) crystallites (Figures 2g,h,k). These results indicated that the morphologies of the birnessites synthesized in concentrated NaOH, using

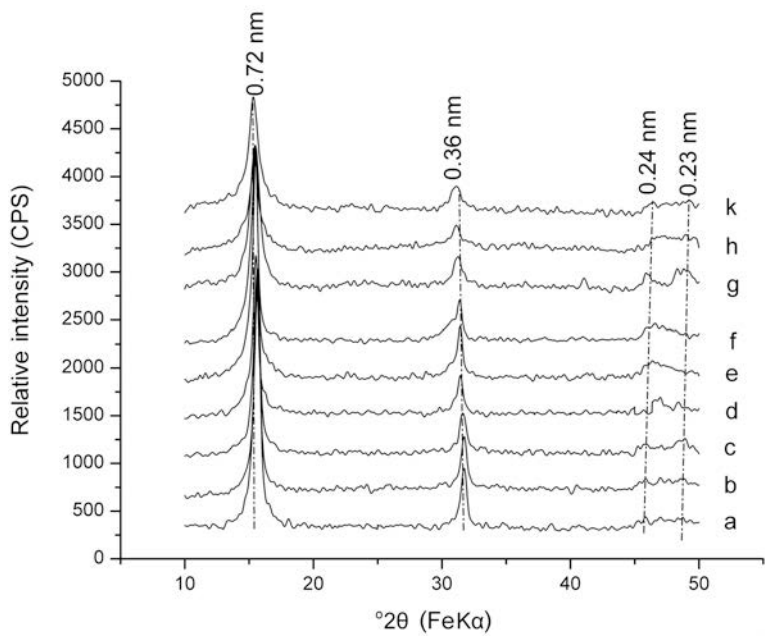

Figure 1. XRD patterns of the synthetic birnessite samples: (a) 0.33-Na(K)-bir; (b) 0.45-Na(K)-bir; (c) 0.55-Na(K)-bir; (d) 0.33-Na-bir; (e) 0.45-Na-bir; (f) 0.55-Na-bir; (g) 0.33-K-bir; (h) 0.45-K-bir; and (k) 0.55-K-bir.

https://doi.org/10.1346/CCMN.2009.0570605 Published online by Cambridge University Press

Table 1. Birnessite synthesis reaction conditions, elemental composition, and average manganese oxidation state (AOS).

Reaction condition	Ratio of MnO_4^-/Mn^{2+}	Sample	Na (mmol/g)	K (mmol/g)	Mn (mmol/g)	AOS
$KMnO_4$+NaOH+$MnCl_2$	0.33	0.33-(Na,K)-bir	3.06	0.13	8.47	3.51
$KMnO_4$+NaOH+$MnCl_2$	0.45	0.45-(Na,K)-bir	3.25	0.16	8.32	3.63
$KMnO_4$+NaOH+$MnCl_2$	0.55	0.55-(Na,K)-bir	3.05	0.31	7.83	3.76
$NaMnO_4$+NaOH+$MnCl_2$	0.33	0.33-Na-bir	3.09		8.67	3.53
$NaMnO_4$+NaOH+$MnCl_2$	0.45	0.45-Na-bir	2.99		8.03	3.80
$NaMnO_4$+NaOH+$MnCl_2$	0.55	0.55-Na-bir	3.12		7.91	3.87
$KMnO_4$+KOH+$MnCl_2$	0.33	0.33-K-bir		0.61	10.23	3.50
$KMnO_4$+KOH+$MnCl_2$	0.45	0.45-K-bir		1.11	9.93	3.61
$KMnO_4$+KOH+$MnCl_2$	0.55	0.55-K-bir		0.90	9.11	3.89

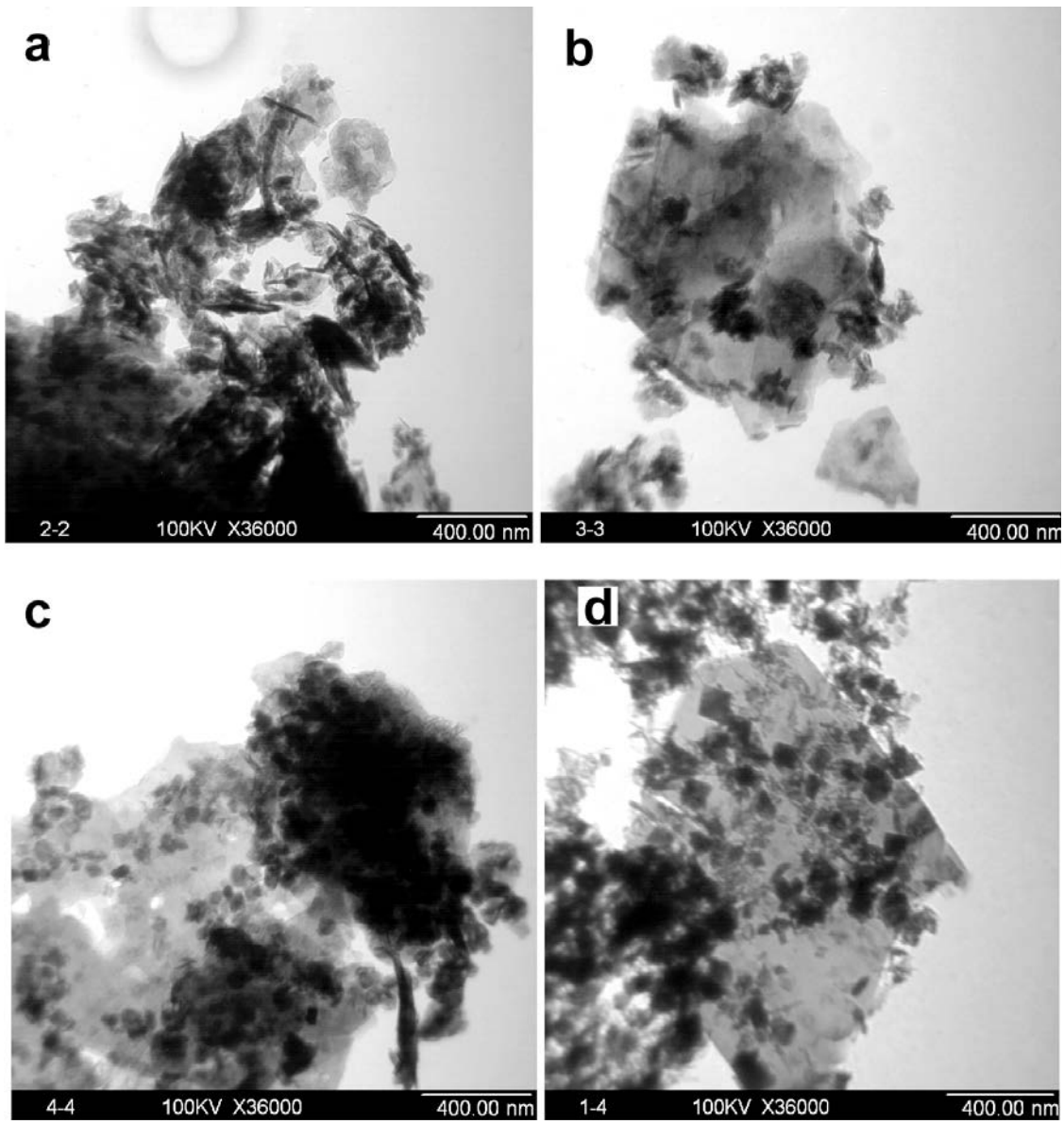

Figure 2 (*above and facing page*). TEM images of the synthetic birnessite samples: (a) 0.33-Na(K)-bir; (b) 0.45-Na(K)-bir; (c) 0.55-Na(K)-bir; (d) 0.33-Na-bir; (e) 0.45-Na-Bir; (f) 0.55-Na-bir; (g) 0.33-K-bir; (h) 0.45-K-bir; and (k) 0.55-K-bir.

https://doi.org/10.1346/CCMN.2009.0570605 Published online by Cambridge University Press

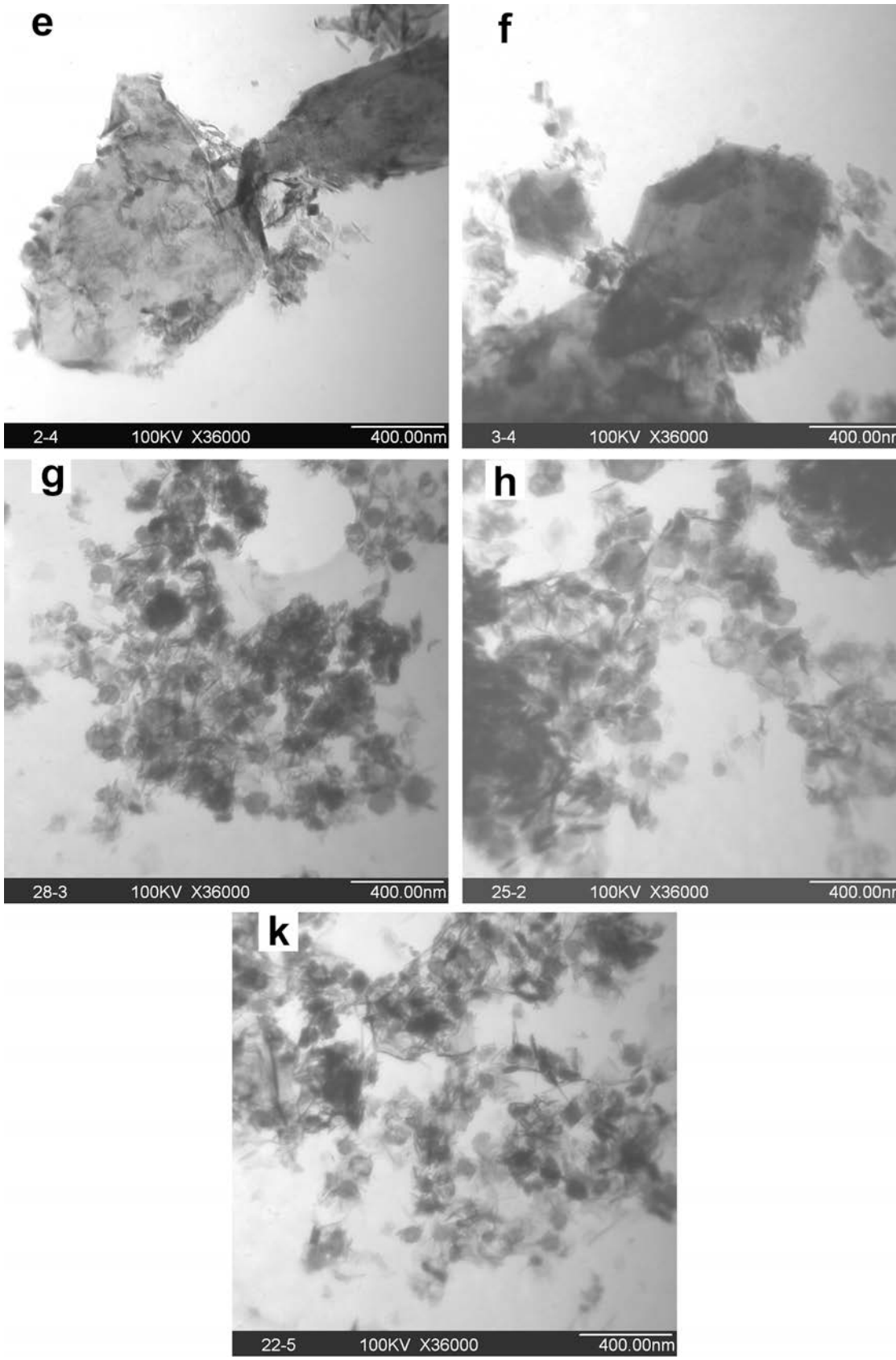

https://doi.org/10.1346/CCMN.2009.0570605 Published online by Cambridge University Press

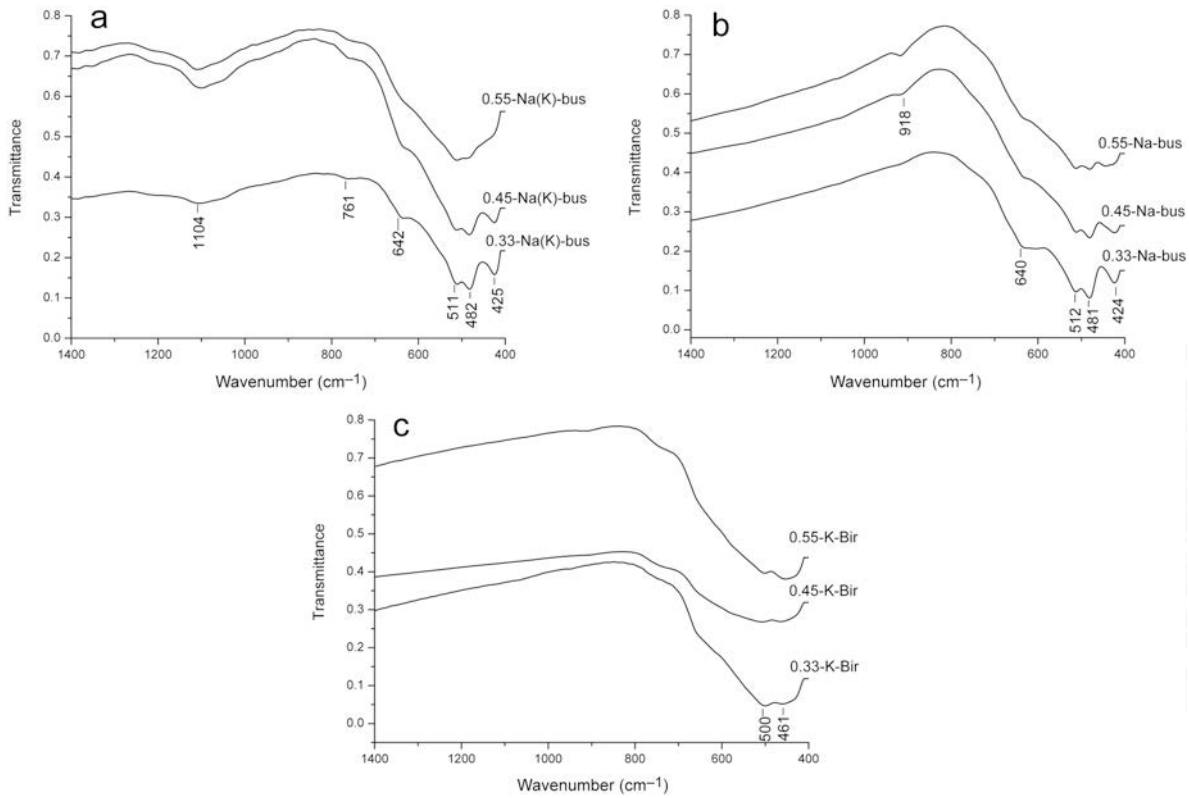

Figure 3. IR spectra of synthetic birnessite samples: (a) Na(K)-birnessite; (b) Na-birnessite; and (c) K-birnessite.

$KMnO_4$ or $NaMnO_4$ as the oxidant, were similar, but birnessites synthesized in concentrated KOH had different morphologies.

The 1400−400 cm^{-1} IR spectra for the synthetic birnessites showed that the (Na,K)-birnessite samples had bands at 1104, 761, 642, 511, 482, and 425 cm^{-1} (Figure 3a). The IR absorption bands at ~511,482, and 425 cm^{-1} are diagnostic for the birnessite structure (Potter and Rossman, 1979; Feng *et al*., 2005; Kang *et al.*, 2007). The synthetic Na-birnessite samples had three IR bands at ~512, 481, and 424 cm^{-1}, in good agreement with the characteristic IR bands for (Na,K)-birnessites. The bands at 1104 and 761 cm^{-1} were not observed for the Na-birnessites, but a new adsorption band near 918 cm^{-1} was observed (Figure 3b). The synthetic K-birnessite samples had IR bands at 500 and 461 cm^{-1} (Figure 3c). The IR spectra indicate that the characteristic absorption band positions differ for

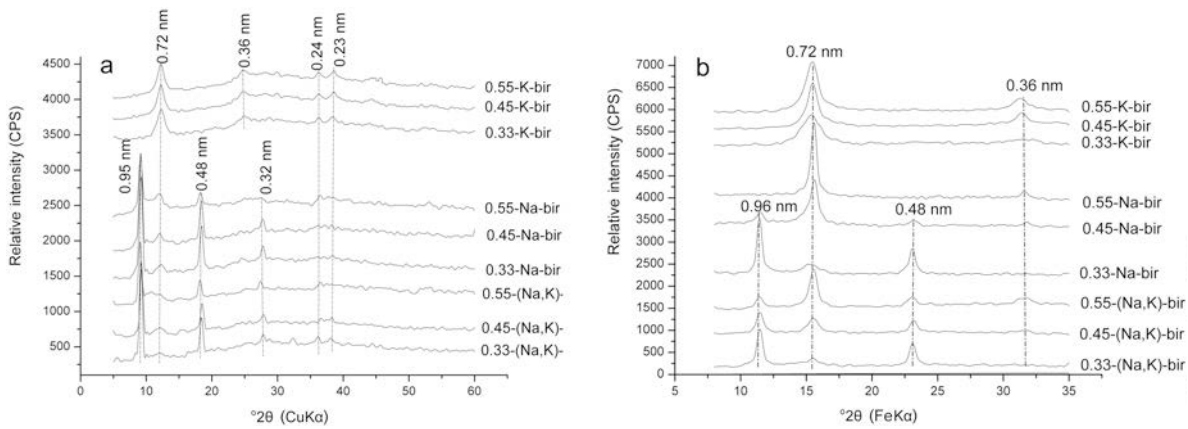

Figure 4. XRD patterns of buserites from ion exchange of birnessites with (a) Mg^{2+} and (b) products of Mg^{2+}-reflux treatment.

https://doi.org/10.1346/CCMN.2009.0570605 Published online by Cambridge University Press

Table 2. Buserite/birnessite elemental composition from Mg^{2+} exchange and average manganese oxidation state (AOS).

Sample	Na (mmol/g)	K (mmol/g)	Mg (mmol/g)	Mn (mmol/g)	AOS
0.33-(Na,K)-bus	0.03	0.09	1.52	8.39	3.50
0.45-(Na,K)-bus	0.03	0.11	1.63	8.27	3.64
0.55-(Na,K)-bus	0.04	0.16	1.57	7.77	3.74
0.33-Na-bus	0.14		1.56	8.58	3.55
0.45-Na-bus	0.14		1.51	7.98	3.78
0.55-Na-bus	0.16		1.60	7.86	3.91
0.33-K-bir		0.60	0.02	10.10	3.52
0.45-K-bir		1.09	0.02	9.87	3.63
0.55-K-bir		0.89	0.03	9.00	3.85

birnessites synthesized under different reaction conditions. For each type of birnessite, the characteristic absorption band positions scarcely change, but the intensities become weaker with greater AOS values. Because the IR bands between 400 and 800 cm^{-1} for the synthetic birnessites can be assigned to Mn-O lattice vibrations, changes in the position and intensity of these characteristic absorption bands could be attributed to changes in the MnO_6 octahedral layer sub-structure.

Buserite formation by Mg^{2+} exchange

A strong 0.95 nm peak and a weak 0.72 nm peak observed in the XRD patterns of (Na,K)- and Na-birnessites exchanged with Mg^{2+} (Figure 4a) indicate that most of the birnessites were converted into buserites because buserite-type manganese oxides characteristically have a 1 nm basal spacing. The Mg^{2+}-exchanged K-birnessite samples had XRD patterns similar to the original K-birnessites, which indicates that the K-birnessites were not converted into buserites (Figures 4a).

The chemical analyses (Table 2) indicate that most of the interlayer Na^+ in (Na,K)-birnessites and Na-birnessites could be replaced by Mg^{2+}. Some of the interlayer K^+ of (Na,K)-birnessites could also be replaced by Mg^{2+}, but most K^+ was retained in the interlayer after Mg^{2+} treatment. The interlayer K^+ content of the K-birnessites was almost unchanged, indicating that the K^+ cations cannot be replaced easily by Mg^{2+}. The Mg-buserite AOS values were similar to the birnessite AOS values.

Formation of todorokite by refluxing reaction

The formation of todorokite was studied using synthetic birnessites with different AOS values and different types of interlayer cations. A strong 0.96 nm todorokite peak and a very weak 0.72 nm birnessite peak appeared in the XRD patterns of the Mg^{2+} refluxing products, formed from precursor birnessites by a Mg^{2+}-templating reaction, revealed that a small amount of birnessite was not converted into todorokite for the 0.33-(Na,K)-bir sample (Figure 4b). When the 0.45-(Na,K)-bir sample was used for todorokite synthesis, the decrease in the 0.96 nm peak intensity was less, whereas the 0.72 nm peak intensity was greater (Figure 4b) indicating that a significant amount of birnessite did not transform into todorokite. The intensity of the 0.96 nm peak for the 0.55-(Na,K)-bir sample was very weak and the 0.72 nm peak was strong (Figure 4b), suggesting that most of the birnessite was not converted into todorokite.

The transformation of the Na-birnessites into todorokite was similar to that for the (Na,K)-birnessite samples (Figure 4b), except that the 0.55-Na-bir sample 0.96 nm peak disappeared and the 0.72 nm peak was intensified (Figure 4b) indicating that the 0.55-Na-bir sample did not transform into todorokite. Only the 0.72 and 0.36 nm peaks were observed in the diffraction patterns of the Mg^{2+} reflux products of the K-birnessite samples (Figure 4b), suggesting that none of the K-birnessite samples was transformed into todorokite. The results suggest decreased todorokite formation at atmospheric pressure with increases in birnessite AOS value and that interlayer K^+ in birnessites was not available for the transformation of birnessite to todorokite.

The TEM bright-field images of the 0.33-(Na,K)-birnessite and 0.33-Na-birnessite reflux products after the Mg^{2+}-templating reaction revealed that fibrous crystals of various lengths extended outward from a platy matrix (Figure 5), a characteristic morphology of todorokite (Cui *et al.*, 2005). A typical HRTEM image obtained for the synthetic todorokite is shown in Figure 6. The lattice fringe spacings were 1.0 nm, which is equivalent to three MnO_6 octahedral chain widths and corresponds to the todorokite [100] structural planes. The TEM and HRTEM images support the XRD results and further confirm that todorokite was formed under refluxing conditions.

The effect of $Na_4P_2O_7$ on birnessite-to-todorokite transformation

Birnessites can contain manganese with oxidation states of 4+, 3+, and 2+. In general, the proportions of Mn^{4+}, Mn^{3+}, and Mn^{2+} in birnessites differ and the AOS values can decrease with increased proportions of Mn^{3+}

https://doi.org/10.1346/CCMN.2009.0570605 Published online by Cambridge University Press

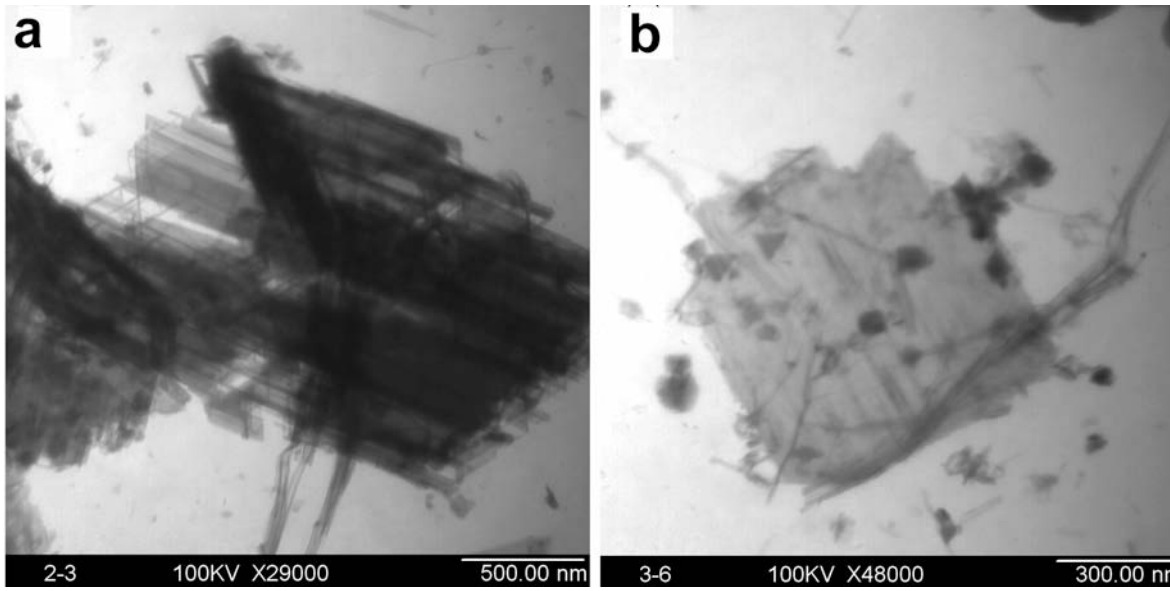

Figure 5. TEM images of (a) 0.33-(Na,K)-birnessite and (b) 0.33-Na-birnessite after Mg^{2+}-reflux treatment.

and Mn^{2+}. Pyrophosphate is a particularly good chelating agent and has been shown to form strong complexes with Mn^{3+}. The Mn^{3+}-pyrophosphate complexes are clear with a red tint (Kostka *et al.*, 1995; Klewicki and Morgan, 1998; Nguyen *et al.*, 2002; Webb *et al.*, 2005).

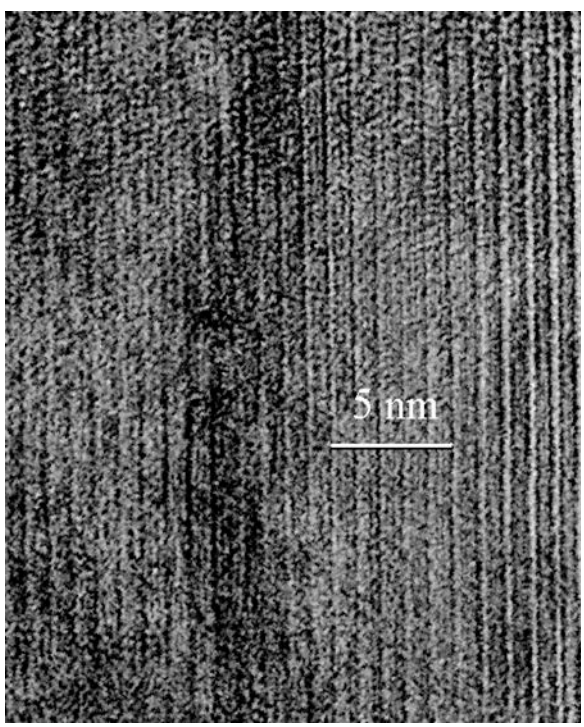

Figure 6. HRTEM image of synthetic todorokite.

After a high AOS-value birnessite sample, 0.55-(Na,K)-bir, was treated with pH 7 0.01 M $Na_4P_2O_7$ and then refluxed with Mg^{2+}, only a 0.72 nm peak was observed in XRD patterns (Figure 7a), indicating that the pyrophosphate-treated birnessite sample was not converted into todorokite. Although the todorokite 0.96 nm peak was present in the Mg^{2+}-refluxing products of pyrophosphate-treated 0.45-(Na,K)-bir and 0.33-(Na,K)-bir samples (Figure 7a), the intensity of the 0.96 nm peak was less than in the Mg^{2+}-refluxed birnessite samples without pyrophosphate pre-treatement (Figure 4b). Three types of birnessite were pre-treated with pH 7 0.02 M $Na_4P_2O_7$ prior to Mg^{2+}-reflux treatment. The 0.96 nm todorokite peak disappeared leaving only the 0.72 nm birnessite peak (Figure 7b). These results indicate that pyrophosphate removal of Mn^{3+} from birnessites inhibited birnessite-to-todorokite transformation during Mg^{2+}-reflux treatment.

DISCUSSION

The transformation of a layered birnessite to a tunnel-structure todorokite is a complex process. Many parameters, such as type and sizes of interlayer cations, amount of interlayer water, and sub-structure of MnO_6 layer, could affect the birnessite-to-todorokite transformation at atmospheric pressure. Although the details of the transformation of birnessite to todorokite are still unclear, the migration of Mn^{3+} may play a crucial role in directing construction of the tunnel structure (Liu *et al.*, 2002; Feng *et al.*, 2004; Liu *et al.*, 2005). The present study indicates that the transformation is closely related to the amounts of Mn^{3+} in birnessites with different AOS

https://doi.org/10.1346/CCMN.2009.0570605 Published online by Cambridge University Press

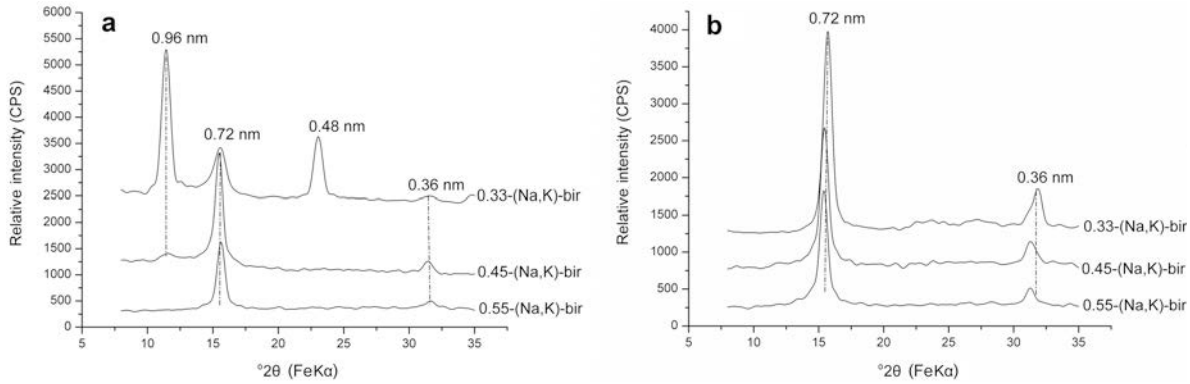

Figure 7. XRD patterns of (Na,K)-birnessites treated with pH 7 0.01 M (a) and 0.02 M (b) $Na_4P_2O_7$ solution before Mg^{2+}-reflux treatment.

values and different interlayer cation types. Birnessites with small AOS values can easily transform to todorokite because many Mn^{3+} are to be found within the structure. However, the transformation does not readily occur for birnessites with large AOS values due to the small amount of Mn^{3+} in the structure. Pyrophosphate treatment of birnessites removed Mn^{3+} from MnO_6 layers to form pyrophosphate complexes in solution and pyrophosphate treatment yielded birnessites with greater AOS values (Table 3). As a result of Mn^{3+} removal, the action of Mn^{3+} in forming the tunnel structure and todorokite was limited (Figure 7). Decreased amounts of Mn^{3+}-pyrophosphate were formed from birnessites with greater AOS values (Figure 8), further suggesting that the amounts of Mn^{3+} in the framework of birnessites with different AOS values are different and greatly influence todorokite formation at atmospheric pressure.

Todorokite has a 1.0 nm d_{001} spacing and commonly forms from *Me*-buserite (*i.e.* birnessites exchanged with different metal cations). However, the interlayer K^+ of (Na,K)-birnessites cannot be completely exchanged with Mg^{2+} (Table 2) and interlayer K^+ inhibits transformation of birnessite to todorokite. Moreover, interlayer K^+ was greater for (Na,K)-birnessites with greater AOS values (Table 2). When K-birnessites were used to prepare todorokite, no todorokite was formed even from birnessites with small AOS values (Figure 4b), suggesting that the formation of todorokite at atmospheric pressure is mainly governed by two factors: the birnessite AOS value and its birnessite interlayer K^+. Such results can be used to examine the mechanisms of formation of todorokite at atmospheric pressure. On the other hand, the criterion for synthesis of manganese-oxide-type octahedral molecular sieves with large tunnel structures is proposed.

Table 3. Average manganese oxidation states (AOS) of (Na,K)-birnessites and (Na,K)-birnessites treated with pH 7 0.01 M (P1) and 0.02 M (P2) $Na_4P_2O_7$.

Sample	AOS	AOS-P1	AOS-P2
0.33-(Na,K)-bir	3.51	3.67	3.78
0.45-(Na,K)-bir	3.64	3.76	3.84
0.55-(Na,K)-bir	3.74	3.83	3.90

SUMMARY

Birnessites with different AOS values were prepared successfully by controlling the MnO_4^-/Mn^{2+} ratio in concentrated NaOH or KOH. The birnessites prepared in NaOH clearly contained both large (500−1000 nm) and small (40−400 nm) plate-shaped crystallites. The birnessites prepared in KOH consisted mostly of irregular (100−200 nm) plate-shaped crystallites. The birnessite-to-todorokite transformation at atmospheric pressure decreased as (Na,K)-birnessite and Na-birnessite AOS values increased from 3.51 to 3.80. No todorokite was formed when a Na-birnessite with an AOS value of 3.87 was used as the precursor. The removal of Mn^{3+} from

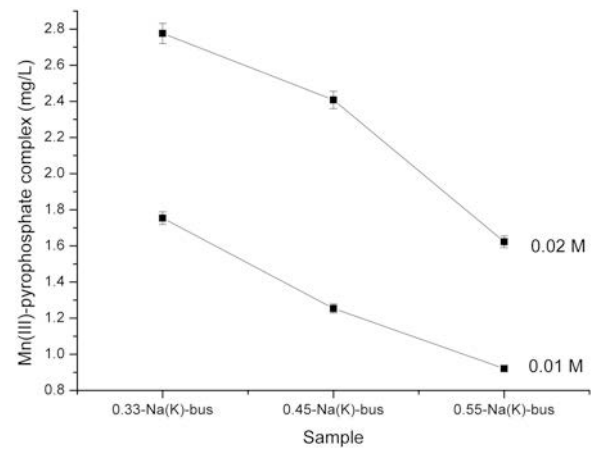

Figure 8. Solution Mn^{3+}-pyrophosphate complex concentrations after three (Na,K)-birnessites with different AOS values were treated with pH 7 0.01 M and 0.02 M pyrophosphate.

https://doi.org/10.1346/CCMN.2009.0570605 Published online by Cambridge University Press

MnO_6 layers by complexation with pyrophosphate solutions limits birnessite to the transformation of todorokite at atmospheric pressure. No (Na,K)-birnessite transformed to todorokite after treatment with pH 7 0.02 M $Na_4P_2O_7$ solution. Interlayer K^+ in (Na,K)-birnessites inhibits todorokite formation and no todorokite was formed from K-birnessites, even from those with small AOS values.

ACKNOWLEDGMENTS

The present study was supported by the National Natural Science Foundation of China (Grant Nos.40771102, Nos. 40830527) and a Foundation for the Author of National Excellent Doctoral Dissertation of China (No. 200767). The authors gratefully acknowledge the associate editor and two anonymous reviewers for their helpful suggestions and for improving the English. They also thank Dr Siebecker Matthew for his help with the final draft and improving the English.

REFERENCES

Al-Sagheer, F.A. and Zaki, M.L. (2004) Synthesis and surface characterization of todorokite-type microporous manganese oxides: implications for shape-selective oxidation catalysts. *Microporous and Mesoporous Materials*, **67**, 43–52.

Cui, H.J., Feng, X.H., Liu, F., Tan, W.F., and He, J.Z. (2005) Factors governing formation of todorokite at atmospheric pressure. *Science in China Series D – Earth Sciences*, **48**, 1678–1689.

Cui, H.J., Feng, X.H., He, J.Z., Liu, F., and Tan, W.F. (2006) Effects of reaction conditions on the formation of todorokite at atmospheric pressure. *Clays and Clay Minerals*, **54**, 605–615.

Cui, H.J., Liu, X.W., Tan, W.F., Feng, X.H., Liu, F., and Ruan H.D. (2008) Influence of Mn(III) availability on the phase transformation from layered buserite to tunnel-structured todorokite. *Clays and Clay Minerals*, **56**, 397–403.

Cui, H., Feng, X., Tan, W., He, J., Hu, R., and Liu, F. (2009) Synthesis of todorokite-type manganese oxide from Cu-buserite by controlling the pH at atmospheric pressure. *Microporous and Mesoporous Materials*, **117**, 41–47.

Feng, X.H., Tan, W.F., Liu, F., Wang, J.B., and Ruan, H.D. (2004) Synthesis of todorokite at atmospheric pressure. *Chemistry of Materials*, **16**, 4330–4336.

Feng, X.H., Tan, W.F., Liu, F., Huang, Q.Y., and Liu, X.W. (2005) Pathways of birnessite formation in alkali medium. *Science in China Series D – Earth Sciences*, **48**, 1438–1451.

Golden, D.C., Chen, C.C., and Dixon, J.B. (1986) Synthesis of todorokite. *Science*,**231**, 717–719.

Golden, D.C., Chen, C.C., and Dixon, J.B. (1987) Transformation of birnessite to buserite, todorokite, and manganite under mild hydrothermal treatment. *Clays and Clay Minerals*, **35**, 271–280.

Kang, L.P., Zhang, M.M., Liu, Z.H., and Ooi, K. (2007) IR spectra of manganese oxides with either layered or tunnel structures. *Spectrochimica Acta Part A*, **67**, 864–869.

Klewicki, J.K. and Morgan, J.J. (1998) Kinetic behavior of Mn(III) complexes of pyrophosphate, EDTA, and citrate. *Environmental Science & Technology*, **32**, 2916–2922.

Kostka, J.E., Luther, III G.W. and Nealson, K.H. (1995) Chemical and biological reduction of Mn(III)-pyrophosphate complexes: Potential importance of dissolved Mn(III) as an environmental oxidant. *Geochimica et Cosmochimica Acta*, **59**, 885–894.

Kumagai, N., Komaba, S., Sakai, H., and Kumagai, N. (2001) Preparation of todorokite-type manganese-based oxide and its application as lithium and magnesium rechargeable battery cathode. *Journal of Power Sources*, **97–98**, 515–517.

Liu, J., Cai, J., Son, Y.C., Gao, Q., Suib, S.L., and Aindow, M. (2002) Magnesium manganese oxide nanoribbons: synthesis, characterization, and catalytic application. *The Journal of Physical Chemistry B*, **106**, 9761–9768.

Liu, Z.H., Kang, L., Ooi, K., Makita, Y., and Feng, Q. (2005) Studies on the formation of todorokite-type manganese oxide with different crystalline birnessite by Mg^{2+}-templating reaction. *Journal of Colloid and Interface Science*, **285**, 239–246.

Luo, J., Zhang, Q., Huang, A., Giraldo, O., and Suib, S.L. (1999) Double-aging method for preparation of stabilized Na-buserite and transformations to todorokites incorporated with various metals. *Inorganic Chemistry*, **38**, 6106–6113.

Mellin, T.A. and Lei, G. (1993) Stabilization of 10 Å-manganates by interlayer cations and hydrothermal treatment: Implications for the mineralogy of marine manganese concretions. *Marine Geology*, **115**, 67–83.

Nguyen, M., Quemard, A., Broussy, S., Bernadou, J., and Meunier, B. (2002) Mn(III) pyrophosphate as an efficient tool for studying the mode of action of Isoniazid on the InhA protein of Mycobacterium tuberculosis. *Antimicrobial Agents and Chemotherapy*, **46**, 2137–2144.

Post, J.E. (1999) Manganese oxide minerals: Crystal structures and economic and environmental significance. *Proceedings of the National Academy of Sciences of the United States of America*, **96**, 3447–3454.

Potter, R.M. and Rossman, G.R. (1979) The tetravalent manganese oxides: identification, hydration, and structural relationships by infrared spectroscopy. *American Mineralogist*, **64**, 1199–1218.

Shen, Y.F., Zerger, R.P., DeGuzman, R.N., Suib, S.L., McCurdy, L., Potter, D.I., and O'Young, C.L. (1993) Manganese oxide octahedral molecular sieves: preparation, characterization, and applications. *Science*, **260**, 511–515.

Shen, Y.F., Suib, S.L., and O'Young, C.L. (1994) Effects of inorganic cation templates on octahedral molecular sieves of manganese oxide. *Journal of the American Chemical Society*, **116**, 11020–11029.

Turner, S., Siegel, M.D., and Buseck, P.R. (1982) Structural features of todorokite intergrowths in manganese nodules. *Nature*, **296**, 841–842.

Webb, S.M., Dick, G.J., Bargar, J.R., and Tebo, B.M. (2005) Evidence for the presence of Mn(III) intermediates in the bacterial oxidation of Mn((II). *Proceedings of the National Academy of Sciences of the United States of America*, **102**, 5558–5563.

Zhou, H., Wang, J.Y., Chen, X., O'Young, C.L., and Suib, S.L. (1998) Studies of oxidative dehydrogenation of ethanol over manganese oxide octahedral molecular sieve catalysts. *Microporous and Mesoporous Materials*, **21**, 315–324.

(*Received 1 December 2008; revised 6 July 2009; Ms. 239; A.E. W.F. Jaynes*)